# PARALLEL MESH REFINEMENT WITHOUT COMMUNICATION

Philippe P. Pébay David C. Thompson

*Sandia National Laboratories*
*Livermore, CA, U.S.A.*

[pppebay,dcthomp]@ca.sandia.gov

## ABSTRACT

This paper presents a technique for the adaptive refinement of tetrahedral meshes. What makes it unique is that no neighbor information is required for the refined mesh to be compatible everywhere. Refinement consists of inserting new vertices at edge midpoints until some tolerance (geometric or otherwise) is met. For a tetrahedron, the six edges present $2^6 = 64$ possible subdivision combinations. The challenge is to triangulate the new vertices (i.e., the original vertices plus some subset of the edge midpoints) in a way that neighboring tetrahedra always generate the same triangles on their shared boundary. A geometric solution based on geometric properties (edge lengths) was developed previously, but did not account for geometric degeneracies (edges of equal length). This paper provides a solution that works in all cases.

**Keywords: Adaptive Tetrahedral Tessellation, Parallel Mesh Refinement, Streaming Subdivision**

## 1. INTRODUCTION

Finite element techniques that use higher order (*i.e.*, nonlinear) polynomial maps, $\Phi : R \longrightarrow F$ and $\Xi : R \longrightarrow X$, from some parametric space, $R$, into the model's geometric space, $X$, and solution space, $F$, of some set of differential equations are becoming more common. Although visualization techniques that use $\Phi$ and $\Xi$ directly are under development, being able to take advantage of the huge number of techniques aimed at linear maps is highly desirable. We propose to do this through an adaptive simplicial tessellation of the parameter space, $R$, into regions where $\Phi$ and/or $\Xi$ are approximately linear. Specifically, this paper describes a subdivision scheme based on error metrics evaluated at edge midpoints of some initial (crude) tessellation, as shown in Figure 1.

This is not the first time adaptive tessellation using edge-based subdivision has been considered; however, other methods either

- work on triangles but not tetrahedra [1, 2],
- produce incompatible mesh elements [3], or
- require neighborhood information and storage space to hash shared output geometry[3, 4].

Since we require a volumetric model for visualizations such as volume rendering, adaptive triangulations that only produce simplicial complexes in lower dimensions are inadequate. Collections of simplices that do not meet the requirements of a simplicial complex are insufficient since algorithms such as isosurfacing will produce inconsistent output. Hashing output geometry so that simplices share common vertices, edges, and faces can require storage on the order of the size of the output and, more importantly, can require communication between processes when tessellation is performed in parallel. In cases where higher order finite elements are being rendered for visualization and not analyzed, the subdivided simplices are not ever stored – they are sent to a graphics card for immediate rendering via OpenGL. Because OpenGL does not require output geometry to share vertices, it is a waste of resources

to spend time insuring the subdivided simplices are in a shared form. This is especially true for view-dependent rendering techniques, where a tessellation of the mesh is produced for each frame rendered.

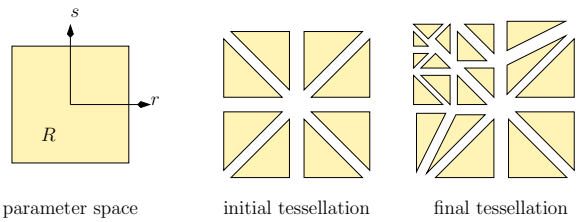


**Figure 1**: Given some initial tessellation of a finite element's parameter space, we subdivide edges until some error metric is met and we are left with a new, refined simplicial complex.

## 1.1 Streaming Subdivision

Given an initial tessellation of an element's parametric domain, we apply an adaptive triangulation technique similar to [2], [1], and [3]. The main difference between our technique and the first two is that we handle tetrahedra as well as triangles and currently use chord error at the parametric midpoint of each edge rather than the angle between normal vectors at each endpoint. Our approach is a direct extension of [3], but insures compatibility in all conditions without neighborhood information. As with the previous work, we assume that the initial tessellation is fine enough that no large changes in the error metric occur interior to the simplices; the adaptive tessellation is intended to improve detail, not capture large changes.

The key design point of our implementation is that there are two tasks performed by an edge-subdivision based tessellation algorithm:

1. making a decision about whether an edge should be subdivided, and
2. applying a template to produce new elements based on which edges of an initial template require subdivision.

We split these two tasks into separate C++ classes so that the same templates for subdivision could be applied to many different subdivision decision algorithms. The algorithms that decide whether edges require subdivision vary depending on

1. the interpolation algorithm used for the nonlinear function,
2. the criteria used in the decision (geometric distance, scalar field nonlinearity),
3. the purpose of the overall task requiring a tessellation.

Item 3 requires some further explanation; if the tessellation is being produced simply for display purposes, then a view-dependent subdivision may be performed. This greatly reduces the amount of work required, since no function evaluation need take place if both edge endpoints are safely outside the viewing frustum[1]. On the other hand, if the tessellation is produced as input to some further post-processing step, then no regions may be excluded from the calculation.

The templates that produce new simplices given a starting simplex $\sigma$ and the edges of $\sigma$ requiring subdivisions deserve some discussion. The problem of triangulating the new set of points (*i.e.*, the original vertices of $\sigma$ and the mid-edge nodes being introduced by the subdivision) is not unique – there may be 1 or many possible triangulations of the point set. With a streaming algorithm, we must guarantee that each simplex may be processed without any information on its neighbors. Since we want to maintain a compatible tessellation, this means that any simplices that are shared as a boundary between two higher-dimensional simplices must be tessellated identically when all the higher-dimensional simplices are divided, even where there are several distinct tessellations. For example, any triangle, $\tau$, shared by two tetrahedra, $\sigma_0$ and $\sigma_1$, must be tessellated the same way when $\sigma_0$ and $\sigma_1$ are subdivided.

[3] developed a method for deciding on a subdivision template so that adjacent simplices produced compatibly-tessellated boundaries. Their technique chooses triangulations that have the best aspect ratios. Unfortunately, they offer no solution when several tessellations exist and have identical aspect ratios. The next two sections review and extend [3] to handle even these cases.

## 1.2 Unambiguous Cases

We use the same nomenclature as [3], so this section is just a brief review of their results. When a tetrahedron, $\sigma$, is to be subdivided, we are given a list of edges of $\sigma$ that will be divided. First, the vertices of $\sigma$ are permuted into $\sigma'$, a positive arrangement of $\sigma$ that matches one of 12 cases ([3] present 11 cases but we divide their case 3c into 3c and 3d so that $\sigma'$ will always be a *positive* arrangement of $\sigma$). Cases are called out with

- the number of edges of a tetrahedron, $\sigma$, that should be subdivided, and
- a letter representing a unique configuration of those edges relative to each other.

Then, a collection of points, $P$, is created that includes $\sigma'$ and the midpoints of edges in $\sigma'$ that must be sub-

[1] We assume that some safety margin is included so that edges which curve into the frustum are not excluded.

divided. This set of points, $P$, must be tessellated in a consistent manner so that simplices adjacent to $\sigma$ will be compatible at the boundary they share with $\sigma$. Let's say we can produce such a tessellation. Call it $\sigma''$. For each of the 12 cases, there will be edges in $\sigma''$ that are constrained to be present and possibly some edges of $\sigma''$ that are not constrained. [3] use geometry – the length of the edges of $\sigma'$ – to decide how to connect points in $P$ to form $\sigma''$. They choose edges for $\sigma''$ that produce tetrahedra with the best possible aspect ratio given $P$. Each case with unconstrained edges in $\sigma''$ will have several variants based on which edges of $\sigma'$ are longer than the others (relative to which edges must be subdivided). Figure 2 shows all 6 variants for Case 3a.

Unfortunately, when edges of $\sigma'$ are of equal length, the edge length criterion gives no answer for how $\sigma''$ should be obtained. This leaves several possibilities for $\sigma''$ and it is ambiguous which one we should use so that $\sigma''$ remains compatible with its neighbors.

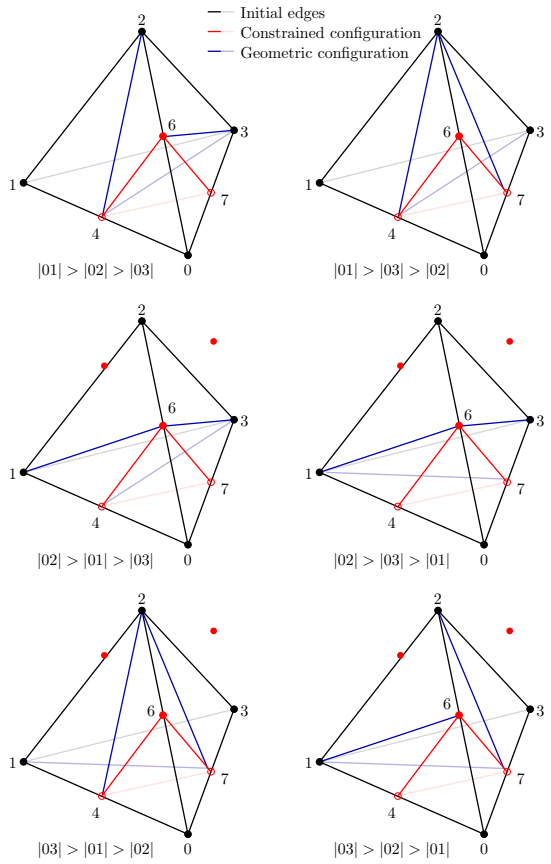


**Figure 2**: Subdivision of unambiguous case 3a.

## 2. AMBIGUOUS CASES

Ambiguous cases occur when a face can be split in two different ways, *i.e.*, whenever at least one face has exactly two edges of equal length that must be split. A simple enumeration shows that all such situations can be summarized by the means of reference configurations 2a, 3a, 3c, 4a, 4b or 5 (see Figure 3).

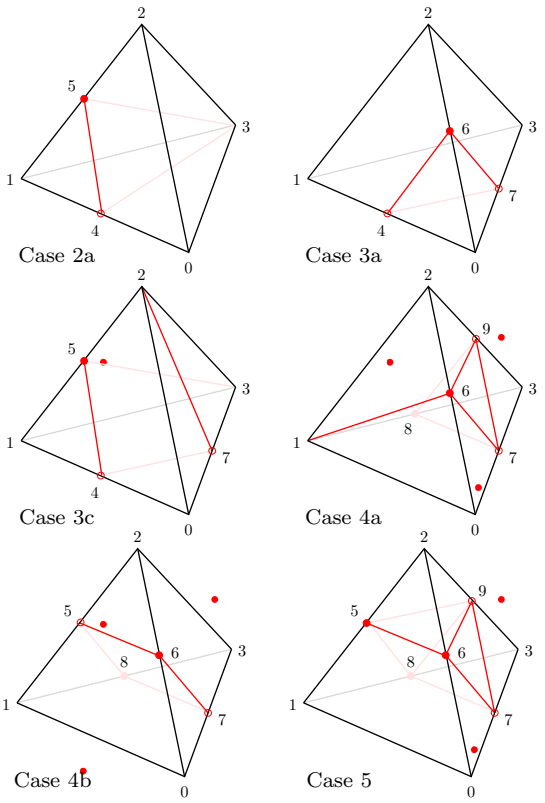


**Figure 3**: Potentially ambiguous configurations.

To resolve the ambiguity when edges of $\sigma'$ are of equal length, we propose adding a new point, $a$, to each face with an ambiguous triangulation. More precisely, the face must be split unequivocally into a triangle and an isosceles trapezoid, the latter having two possible triangular subdvisions, both of them being acceptable according to the subdivision algorithm (*cf.* Figure 4(a)). By placing $a$ on the angle bisector of the vertex opposite the base of the trapezoid, as shown in Figure 4(b), there exists a triangulation that is symmetric about the angle bisector and will be identical for $\sigma$ and any tetrahedron that shares the face with $\sigma$. The exact placement of $a$ on the angle bisector for the best resulting tetrahedra is unclear. Hence, two questions must now be addressed: where to put the point, and, once the point has been placed, how to decompose the tetrahedron. We are now proposing answers to both questions.

### 2.1 The Point and Where to Put It

Because the point placement method must be designed such that the same point is found when applied from either of the elements sharing the ambiguous face, the

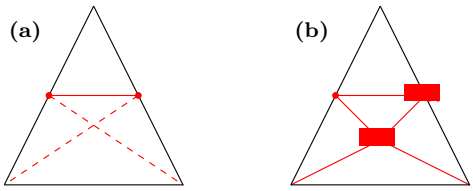


**Figure 4**: Ambiguous isosceles face refinement: (a) two different subdivisions are possible, and (b) unambiguous subdivision thanks to a point insertion.

point must necessarily be inserted on the orthogonal bisector of the nonsplit edge (which is also the median and the angle bisector, because the face is isosceles), as illustrated in Figure 4(b). Therefore, topologically speaking, the point may be placed anywhere on the open segment of this edge bisector contained in the interior of the iscosceles trapezoid. However, geometrically speaking, not all placements are the same, since triangle quality will vary, which will in turn have an effect on tetrahedral quality [5]. We will measure quality using the normalized edge to inradius triangle quality measure $\zeta$, defined as follows:

$$\zeta_t = \frac{p}{3\sqrt{3}r},$$

where $p$ and $r$ respectively denote the semiperimeter and the inradius of the triangle $t$ to be evaluated. Thanks to the normalization factor one always has $\zeta_t \geq 1$, with equality if and only of the triangle is equilateral. For the sake of our specific needs, we will use the angle formulation derived in [6]:

$$\zeta(\alpha,\beta) = \frac{(\sin\alpha + \sin\beta + \sin(\alpha+\beta))^2}{6\sqrt{3}\sin\alpha\sin\beta\sin(\alpha+\beta)}, \qquad (2.1)$$

where $\alpha$ and $\beta$ denote any two (nonoriented) angles of the triangle.

*Remark* 2.1. In fact, $\zeta$ is the symmetrized aspect-ratio, in the sense that the aspect-ratio is generally defined as the quotient of the largest edge length to the inradius (*cf.* [5]). However, the latter lacks symmetry, and therefore lacks a smooth behavior around its *optimum* and is less convenient to handle algebraically. Replacing the largest edge length with the semiperimeter (rather than the perimeter for more convenient algebraic formulas) solves both issues. See [6] for more details on this matter.

Without loss of generality, we now assume that the ambiguous face is 012, isosceles at vertex 2, with 12 and 02 having to be split with their respective midpoints 5 and 6; all other ambiguous cases can be deduced from this one by vertex permutation. The (fixed) nonoriented angle $\widehat{012} = \widehat{102}$ is denoted $\alpha$. We evaluate the overall quality of the subdivision by simply taking the arithmetic mean of the $\zeta$ qualities of the

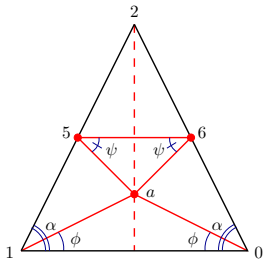


**Figure 5**: Point placement in the isotrapezoid case (in the case of face 012 with $|02| = |12|$).

triangles subdviding the isotrapezoid, that therefore depends solely on the additional point $a$ be inserted, as follows:

$$\overline{\zeta}(a) = \frac{\zeta_{a06} + \zeta_{a65} + \zeta_{a51} + \zeta_{a10}}{4}. \qquad (2.2)$$

Since $a$ must be inserted on the orthogonal bisector of the nonsplit edge and in the interior of the isosceles triangle, it is uniquely determined by the knowledge of $\phi = \widehat{01a} = \widehat{10a}$; for the sake of simplicity, we set $\psi = \widehat{56a} = \widehat{65a}$ (see Figure 5). Denoting $x$ the distance between edge 01 and point $a$, elementary trigonometric considerations show that $0 < x < \frac{1}{2}\sin\alpha = x_{\max}$. It thus immediately follows that

$$\phi = \arctan\frac{x}{\cos\alpha}, \qquad (2.3)$$

$$\psi = \arctan\frac{2(x_{\max} - x)}{\cos\alpha}, \qquad (2.4)$$

and $2\tan\phi + \tan\psi = \tan\alpha$. We can now express $\overline{\zeta}$ in angular terms, by combining (2.1) with (2.2):

$$\overline{\zeta}(\phi,\psi) = \frac{\zeta(\phi,\phi) + \zeta(\psi,\psi) + 2\zeta(\alpha-\phi,\phi+\psi)}{4}.$$

Thanks to (2.3) and (2.4), $\overline{\zeta}(\phi,\psi)$ can thus be uniquely determined by the knowledge of $x$ ($\alpha$ being fixed). We therefore provide numerical plots of $\overline{\zeta}$ for various values of $\alpha$ in Figure 6; the abscissa displays $\frac{x}{x_{\max}}$ rather than $x$ since $x_{\max}$, and thus the range of $x$, varies with $\alpha$, and it is more useful to consider the relative position of $a$ along the bissector than its absolute placement.

Figure 6 clearly shows that the optimal $\zeta$-position of $a$ varies with $\alpha$; in particular, none of the intuitively best placements (either $\frac{1}{2}$ or $\frac{2}{3}$, the latter corresponding to the diagonals intersection, as easily shown by Thales' Theorem) turns out to be optimal in general.

**Example 2.2.** With $\alpha = \frac{\pi}{6}$, the average $\zeta$-quality is *ca.* 3.02896 and 4.07374 with respective relative positions of $\frac{1}{2}$ and $\frac{2}{3}$, while we can attain 2.95994 with $\frac{x}{x_{\max}} = \frac{16}{3}$.

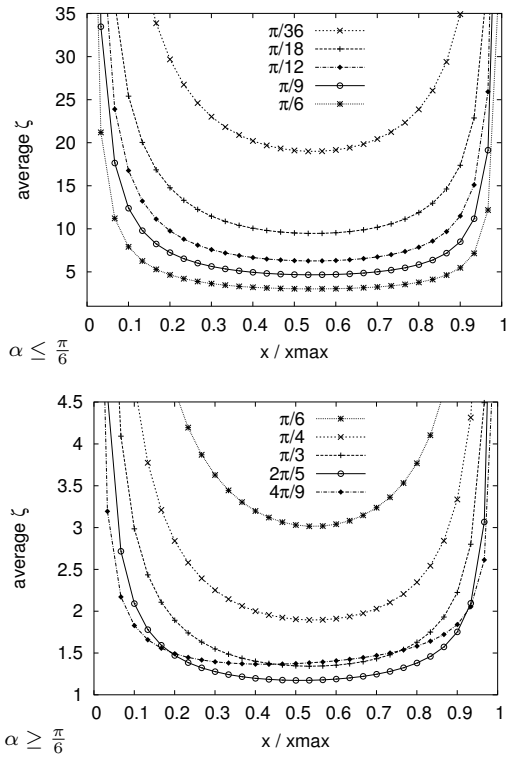


**Figure 6**: Average $\zeta$-quality of the decomposition depending on the point placement, for various values of $\alpha$.

However, establishing an anlytical *optimum*, if feasible, seems to be at least extremely complicated. For the time being, and since this seems to provide an approximation that is "good enough", we choose to insert $a$ at $\frac{1}{2}x_{\max} = \frac{1}{4}\sin\alpha$.

*Remark* 2.3. It shall be acknowledged that this choice for $a$ is *not* of the diagonals intersection; in particular, the subdivided triangles do not have colinear edges.

We do not discuss here the influence over the tetrahedral quality, since it depends on a fourth vertex; however, as explained in [5], good face quality helps to achieve good element quality.

## 2.2 Element Subdivision

We will now categorize and resolve all the ambiguities for each ambiguous case. Where a face needs an additional point, we use a letter to reference that point. We use the letter $a$, $b$, $c$, or $d$ for the point on face 012, 031, 132, or 023, respectively. Note that the position of this point depends on which edges of that face are subdivided, but this is always unequivocal since at most one additional point per face is required. Each subcategory is called out with a Greek letter appended to the index and letter of the ambiguous case from which it derives.

**Case 2a** Case 2a becomes equivocal when $|01| = |12|$, with the ambiguous face 012 that requires a point insertion to remove the ambiguity. By inserting a new vertex, we produce a subdivision of the triangle that is symmetric (*cf.* Figure 12(a)).

**Case 3a** Edges to be split are 01, 02 and 03, and therefore ambiguities arise if and only if at least two of them have the same lengths (see Figure 7). If exactly two of these edges have same length, then the third one might be either shorter or longer. Hence, $1 + \binom{2}{2} \times 2 = 7$ ambiguous configurations may arise. But, up to a vertex permutation, those can be summarized with only three cases: $|01| = |02| > |03|$ (case 3a$\alpha$), $|01| = |02| < |03|$ (case 3a$\beta$), and $|01| = |02| = |03|$ (case 3a$\gamma$).

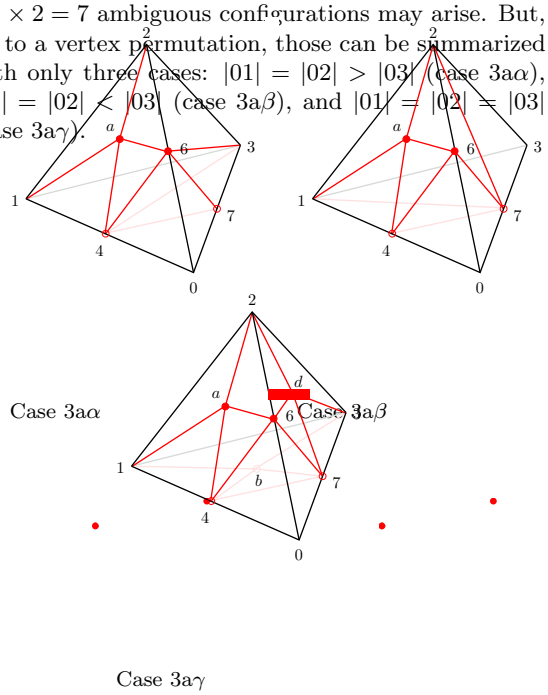


**Figure 7**: Ambiguous configurations of case 3a.

**Case 3c** As shown in Figure 8, edges to be split are 01, 12 and 03, whence only faces 012 and 031 can have equivocal decompositions. One possibility is that exactly one face decomposition is ambiguous, which means that either $|01| = |12|$ and $|12| \neq |03|$, or $|12| = |03|$ and $|01| \neq |12|$. Depending on whether $\neq$ is indeed $<$ or $>$, these $2 \times 2 = 4$ configurations are represented, up to vertex permutation, by case 3c$\alpha$ ($|01| = |12| > |03|$) and 3c$\beta$ ($|01| = |12| < |03|$). The other possibility is that both face decompositions are ambiguous, *i.e.* $|01| = |12| = |03|$ (case 3c$\gamma$).

**Case 4a** Three edge midpoints belong to the same face, represented here as 023, that is therefore necessarily unambiguous. The remaining split edge, 13, is shared by faces 013 and 123; each of these faces also has another edge midpoint, so both may be ambiguous. The remaining face, 012, has a unique edge midpoint and is thus unambiguously triangulated. What

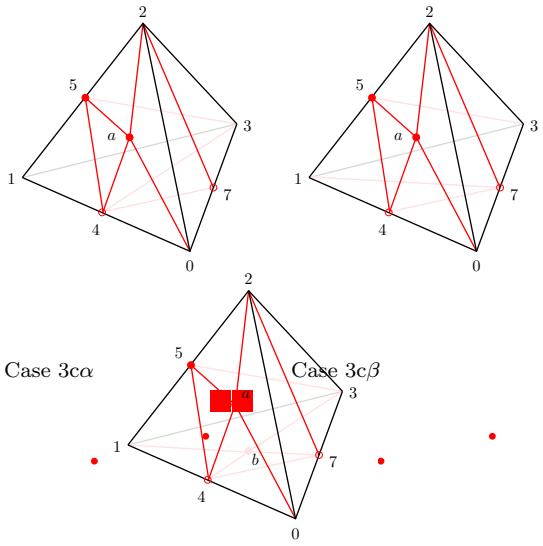


**Figure 8**: Ambiguous configurations of case 3c.

matters here are thus the lengths of 03 and 23 compared to 13, since they decide the fate of the potentially ambiguous faces: |13| may be equal to either one or two of |03| and |23|, which means respectively one or two ambiguous faces. In other words, there are $2 \times 2 + 1 = 5$ ambiguous configurations, that can be represented, up to a vertex permutation, by either 4a$\alpha$ ($|03| = |13| > |23|$), 4a$\beta$ ($|03| = |13| < |23|$), or 4a$\gamma$ ($|03| = |13| = |23|$), see Figure 9.

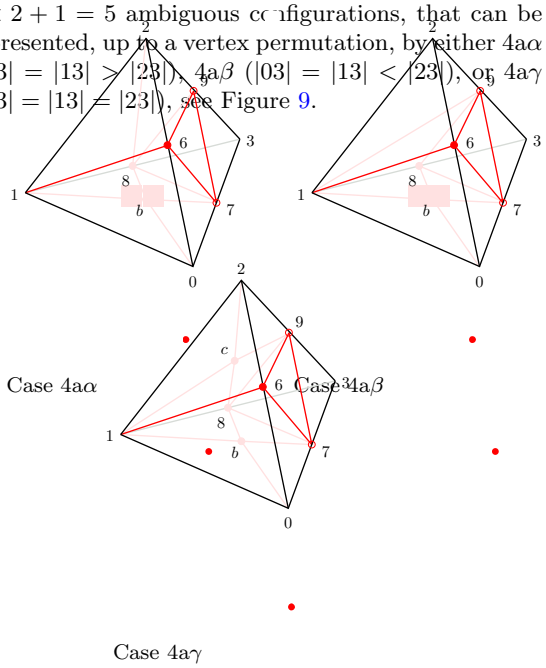


**Figure 9**: Ambiguous configurations of case 4a.

**Case 4b** This case, illustrated in Figure 10, is by far the most complex one: four edge midpoints distributed such that every face contains exactly two of them. Indeed, the distribution of midpoints along a "diametral" path around the tetrahedron allows each face to be ambiguous, and most of such ambiguities may be further refined in subcases, depending on the configuration of unambiguous faces. Again, grouping of topologically equivalent cases may be done, depending on the number, and respective positions, of ambiguous faces. First, it is interesting to notice that the fate of the faces is solely determined by |02|, |12|, |03| and |13|, the two other edges playing no role here. It is also straightforward to see that one cannot have exactly three ambiguous faces, since having three ambiguous faces means that three distinct pairs of the split edges have the same length, and thus by transitivity that all of these edges have the same length; in other words, four faces are ambiguous. Face 012 will be used as the ambiguous face to represent the class of all configurations with a unique ambiguity; in this case, $|02| = |12|$ and several possibilities are left to the other faces to be split, namely 023, 031 and 132, depending on the values of |03| and |13| relative to $|02| = |12|$. Each of these subcases can be deduced, up to vertex permutation, by either 4b$\alpha$ ($|02| = |12| < |13| < |03|$), or 4b$\beta$ ($|02| = |12| > |13| > |03|$), or 4b$\gamma$ ($|03| < |02| = |12| < |13|$). If exactly two faces are ambiguous, then they are either opposed or adjacent. The former case has a unique topological representation, 4b$\delta$ ($|02| = |12| < |03| = |13|$), and all actual configurations can be deduced thereof, thanks to a vertex permutation. The latter case has a remaining degree of freedom, in the sense that three of the split edges have the same length, and the fourth one can be either shorter or longer; therefore, two configurations will represent all possible subcases: 4b$\epsilon$ ($|02| = |12| = |03| < |13|$), and 4b$\zeta$ ($|02| = |12| = |03| > |13|$). Finally, the unique case with four ambiguous faces is called 4b$\eta$ ($|02| = |12| = |03| = |13|$).

**Case 5** All edges but 01 must be split, and thus only faces 012 and 031 can lead to ambiguities, while faces 132 and 023 are decomposed each into 4 unambiguous subfaces (see Figure 3). Therefore, only 3 ambiguous configurations are possible, depending on whether one (two cases, represented up to a face permutation by configuration 5$\alpha$: $|02| = |12|$ and $|03| > |13|$), or two (one configuration, 5$\beta$: $|02| = |12|$ and $|03| = |13|$) faces are ambiguous (see Figure 11).

As introduced in 2.1, we proposed lifting the above ambiguities by the means of point(s) insertion(s) in the interior of the ambiguous faces. Designing compatible tetrahedral subdivisions for each case is very lengthy and sometimes complex but, *labor omnia vicit improbus*, we have gone through this process. Because of format requirement, we do not detail the actual proofs that these decompositions form simplicial conforming meshes of the original element, but a summary is provided in Table 3. In addition, Figures 12, 13, 14, 15, 16, 17, 18, 19, 20, 21, 22, 23, 24, 25, 26, 27, 28, 29 and 30 provide the reader with an intuitive justification.

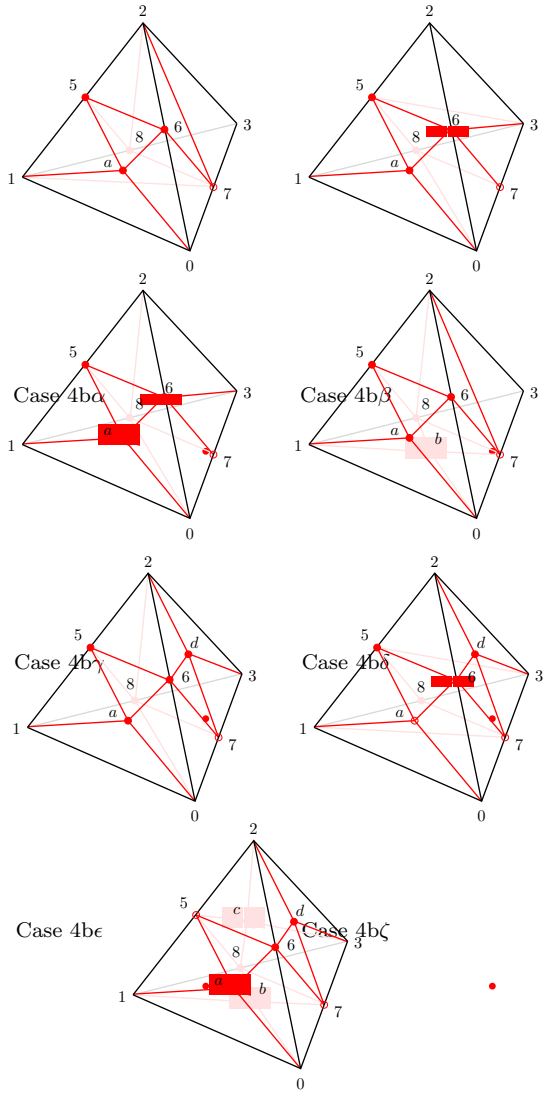


**Figure 10**: Ambiguous configurations of case 4b.

*Remark* 2.4. The decompositions we propose seem to be the most natural ones, displaying decent elements qualities (at least when the initial tetrahedron so does).

## 3. CONCLUSION

We have presented a new scheme for refining tetrahedral meshes that does not require neighborhood information. This makes it viable for streaming large datasets and for parallel processing, where communication would be required to process elements on boundaries between processes.

One property of our proposed technique is that, of the 4 triangles produced by tessellating the isosceles trapezoid, 2 of them will be isosceles triangles. This means that if further subdivisions are required on the two equal-length edges of either isosceles triangle, we will again have an ambiguous case. This is undesirable since detecting the ambiguity and placing point $a$ is slightly more work than handling an unambiguous case.

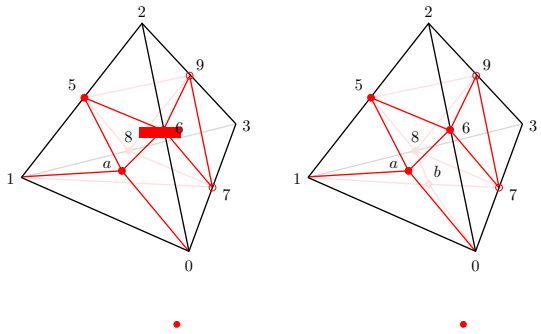


**Figure 11**: Ambiguous configurations of case 5.

Although we have studied the quality of the triangles on tetrahedra produced by ambiguous cases, we have not studied the overall quality of the resulting tetrahedra. This, along with a characterization of the number of tetrahedra required over the unambiguous cases is future work.

## References

[1] Velho L. "Simple and Efficient Polygonization of Implicit Surfaces." *Journal of Graphics Tools*, vol. 1, no. 2, 5–24, 1996

[2] Chung A.J., Field A.J. "A Simple Recursive Tessellator for Adaptive Surface Triangulation." *Journal of Graphics Tools*, vol. 5, no. 3, 2000

[3] Ruprecht D., Müller H. "A Scheme for Edge-based Adaptive Tetrahedron Subdivision." H.C. Hege, K. Polthier, editors, *Mathematical Visualization*, pp. 61–70. Springer Verlag, Heidelberg, 1998

[4] Oliker L., Biswas R., Gabow H.N. "Parallel Tetrahedral Mesh Adaptation with Dynamic Load Balancing." *Parallel Computing Journal, Special Issue on Graph Partitioning*, pp. 1583–1608, 2000

[5] Frey P.J., George P.L. *Mesh Generation*. Hermes Science Publishing, Oxford & Paris, 2000

[6] Pébay P.P., Baker T.J. "Analysis of triangle quality measures." *Mathematics of Computation*, vol. 72, no. 244, 1817–1839, 2003

# APPENDIX: SUBDIVISIONS OF AMBIGUOUS CASES

## Summary

**Table 1**: Subdivisions of ambiguous cases

| Case | Ambiguity | Tetrahedra |
|---|---|---|
| 2a | $\|01\| = \|12\|$ | $04a3$ $0a23$ $4153$ $45a3$ $a523$ |
| 3a$\alpha$ | $\|01\| = \|02\| > \|03\|$ | $0467$ $4367$ $a123$ $a263$ $a643$ $a413$ |
| 3a$\beta$ | $\|01\| = \|02\| < \|03\|$ | $0467$ $1327$ $a127$ $a267$ $a647$ $a417$ |
| 3a$\gamma$ | $\|01\| = \|02\| = \|03\|$ | $0467$ $26ad$ $37db$ $41ab$ $b6a4$ $b6da$<br>$b67d$ $b647$ $2abd$ $1ab2$ $2b3d$ $321b$ |
| 3c$\alpha$ | $\|01\| = \|12\| > \|03\|$ | $4153$ $a047$ $a207$ $a743$ $a273$ $a523$ $a453$ |
| 3c$\beta$ | $\|01\| = \|12\| < \|03\|$ | $7153$ $7523$ $a047$ $a207$ $a527$ $a457$ $1547$ |
| 3c$\gamma$ | $\|01\| = \|12\| = \|03\|$ | $415b$ $b153$ $a047$ $a207$ $a523$<br>$a273$ $a74b$ $a7b3$ $a45b$ $ab53$ |
| 4a$\alpha$ | $\|03\| = \|13\| > \|23\|$ | $7893$ $670b$ $601b$ $6978$ $67b8$ $6b18$ $1268$ $2689$ |
| 4a$\beta$ | $\|03\| = \|13\| < \|23\|$ | $7893$ $670b$ $601b$ $6978$ $67b8$ $6b18$ $1269$ $1689$ |
| 4a$\gamma$ | $\|03\| = \|13\| = \|23\|$ | $7893$ $670b$ $601b$ $6978$ $67b8$<br>$6b18$ $612c$ $629c$ $698c$ $681c$ |
| 4b$\alpha$ | $\|02\| = \|12\| < \|13\| < \|03\|$ | $7823$ $a607$ $a158$ $a017$ $a718$<br>$67a8$ $6a58$ $6278$ $6528$ |
| 4b$\beta$ | $\|02\| = \|12\| > \|13\| > \|03\|$ | $6523$ $a607$ $a158$ $a018$ $a708$<br>$67a8$ $6a58$ $6378$ $6538$ |
| 4b$\gamma$ | $\|03\| < \|02\| = \|12\| < \|13\|$ | $6238$ $a607$ $a158$ $a018$ $a708$<br>$67a8$ $6a58$ $6378$ $6528$ |
| 4b$\delta$ | $\|02\| = \|12\| < \|03\| = \|13\|$ | $7823$ $a607$ $a158$ $a01b$ $ab18$ $a0b7$<br>$a7b8$ $67a8$ $6a58$ $6278$ $6528$ |
| 4b$\epsilon$ | $\|02\| = \|12\| = \|03\| < \|13\|$ | $a607$ $a158$ $a018$ $a708$ $d625$ $d378$<br>$d238$ $d285$ $67a8$ $6a58$ $6d78$ $65d8$ |
| 4b$\zeta$ | $\|02\| = \|12\| = \|03\| > \|13\|$ | $a607$ $a158$ $a017$ $a718$ $d625$ $d378$<br>$d235$ $d385$ $67a8$ $6a58$ $6d78$ $65d8$ |
| 4b$\eta$ | $\|02\| = \|12\| = \|03\| = \|13\|$ | $a607$ $a158$ $a01b$ $ab18$ $a0b7$ $a7b8$ $d625$ $d378$<br>$d23c$ $d2c5$ $dc38$ $d5c8$ $67a8$ $6a58$ $65d8$ $6d78$ |
| 5$\alpha$ | $\|02\| = \|12\|, \|03\| > \|13\|$ | $6529$ $7893$ $a607$ $a158$ $a017$<br>$a718$ $a859$ $a789$ $a679$ $a569$ |
| 5$\beta$ | $\|02\| = \|12\|, \|03\| = \|13\|$ | $6529$ $7893$ $a607$ $a158$ $a01b$ $ab18$<br>$a0b7$ $a7b8$ $a859$ $a789$ $a679$ $a569$ |

## Figures

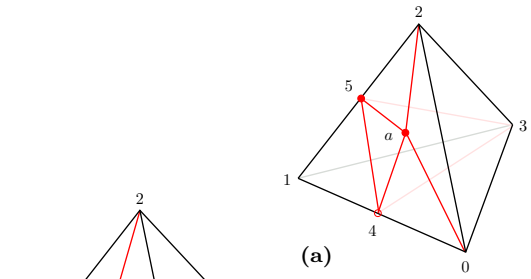


**Figure 12**: Ambiguous case 2a ($|01| = |12|$): (12(a)) constrained configuration, and (12(b)) complete subdivision.

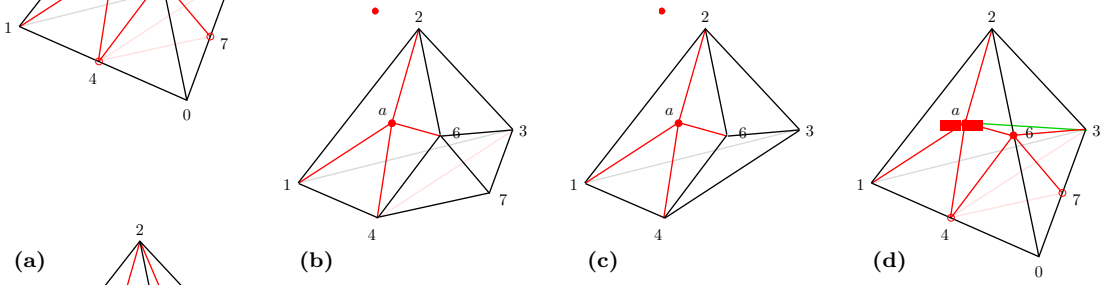


**Figure 13**: Ambiguous case 3a$\alpha$ ($|01| = |02| > |03|$): (13(a)) constrained configuration, (13(b)) after removal of $0467$, (13(c)) after removal of $4367$, and (13(d)) complete subdivision.

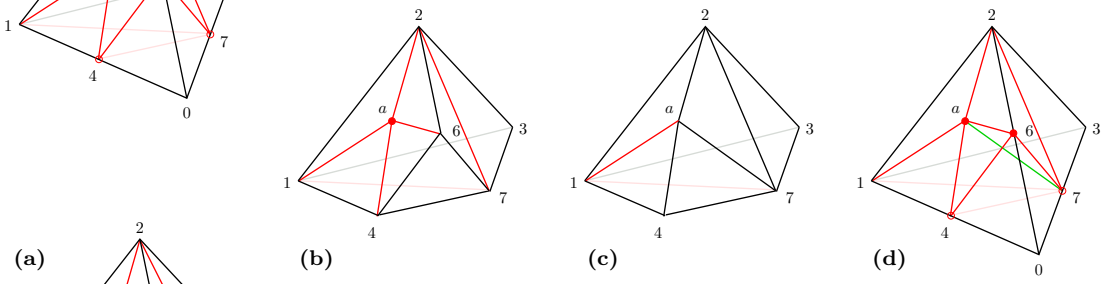


**Figure 14**: Ambiguous case 3a$\beta$ ($|01| = |02| < |03|$): (14(a)) constrained configuration, (14(b)) after removal of $0467$, (14(c)) after removal of $4367$, and (14(d)) complete subdivision.

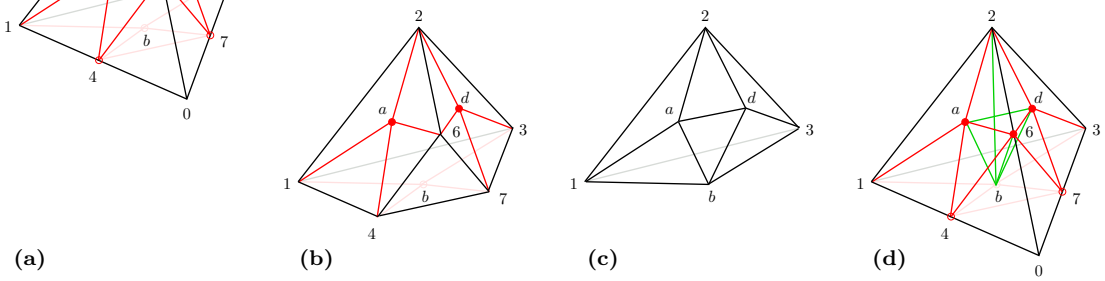


**Figure 15**: Ambiguous case 3a$\gamma$ ($|01| = |02| = |03|$): (15(a)) constrained configuration, (15(b)) after removal of $0467$, (15(c)) after removal of $62d74a$, and (15(d)) complete subdivision.

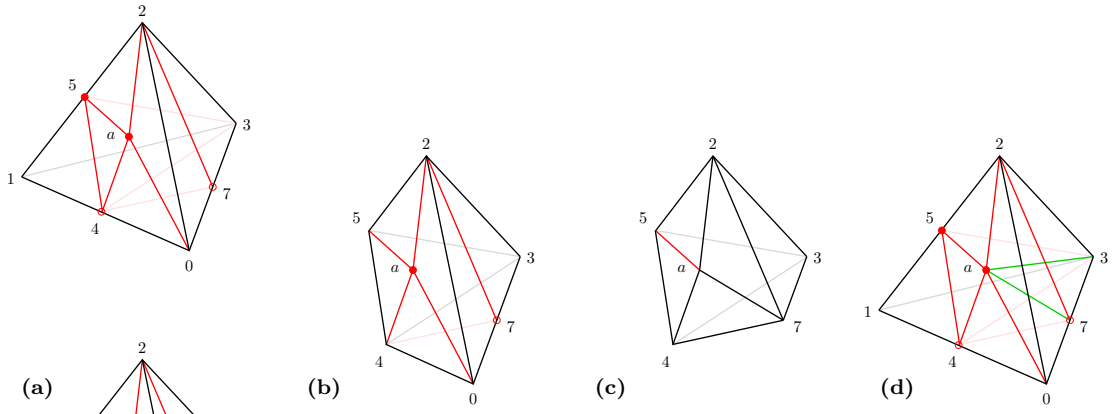


**Figure 16**: Ambiguous case 3c$\alpha$ ($|01| = |12| > |03|$): (16(a)) constrained configuration, (16(b)) after removal of $4153$, (16(c)) after removal of $a047$ and $a207$, and (16(d)) complete subdivision.

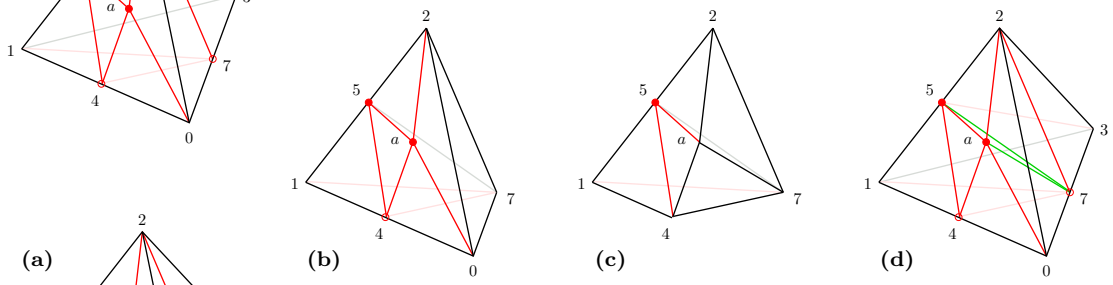


**Figure 17**: Ambiguous case 3c$\beta$ ($|01| = |12| < |03|$): (17(a)) constrained configuration, (17(b)) after removal of $7153$ and $7523$, (17(c)) after removal of $a047$ and $a207$, and (17(d)) complete subdivision.

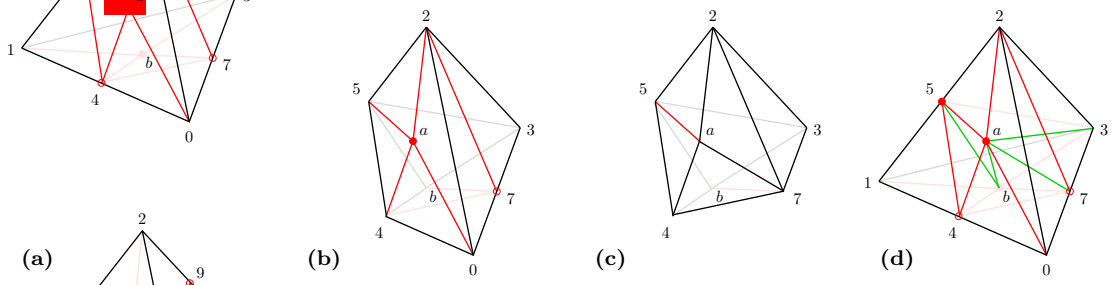


**Figure 18**: Ambiguous case 3c$\gamma$ ($|01| = |12| = |03|$): (18(a)) constrained configuration, (18(b)) after removal of $415b$ and $b153$, (18(c)) after removal of $a047$ and $a207$, and (18(d)) complete subdivision.

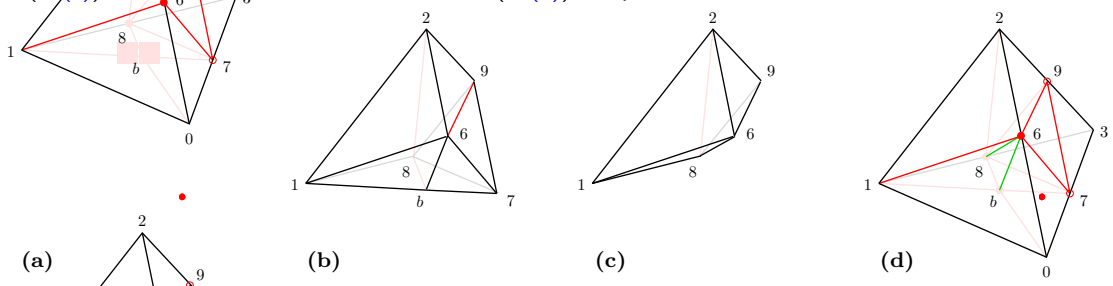


**Figure 19**: Ambiguous case 4a$\alpha$ ($|03| = |13| > |23|$): (19(a)) constrained configuration, (19(b)) after removal of $7893$, $670b$ and $601b$, (19(c)) after removal of $6978$, $67b8$ and $6b18$, and (19(d)) complete subdivision.

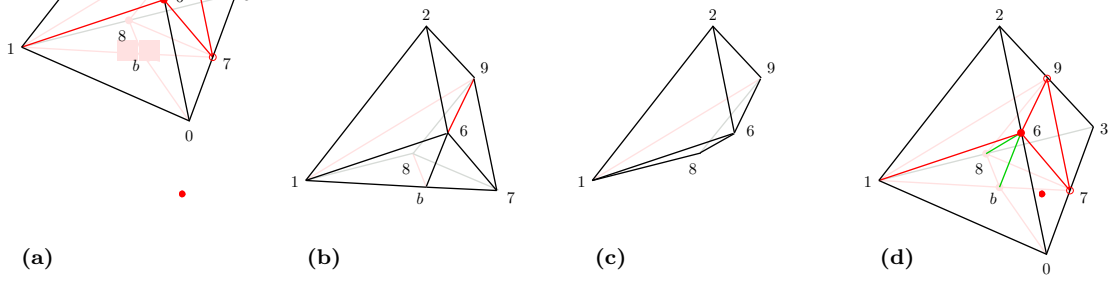


**Figure 20**: Ambiguous case 4a$\beta$ ($|03| = |13| < |23|$): (20(a)) constrained configuration, (20(b)) after removal of $7893$, $670b$ and $601b$, (20(c)) after removal of $6978$, $67b8$ and $6b18$, and (20(d)) complete subdivision.

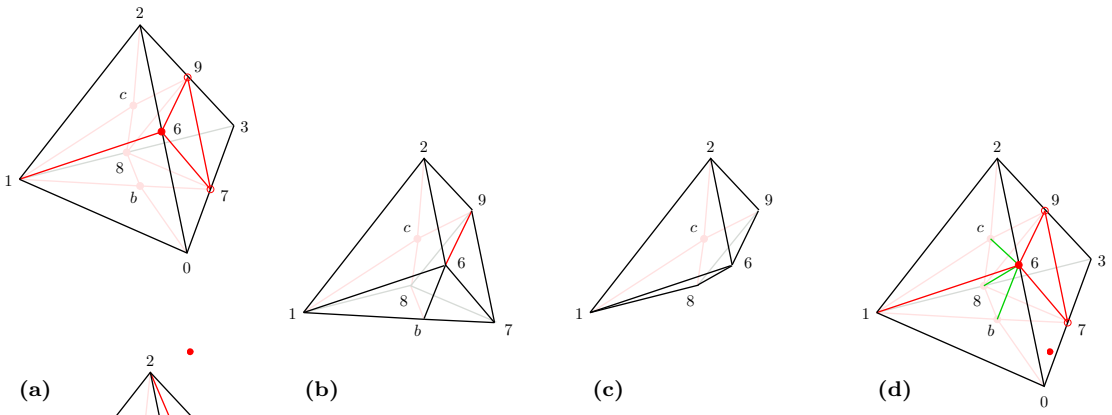


(a) (b) (c) (d)

**Figure 21**: Ambiguous case 4a$\gamma$ ($|03| = |13| = |23|$): (21(a)) constrained configuration, (21(b)) after removal of $7893$, $670b$ and $601b$, (21(c)) after removal of $6978$, $67b8$ and $6b18$, and (21(d)) complete subdivision.

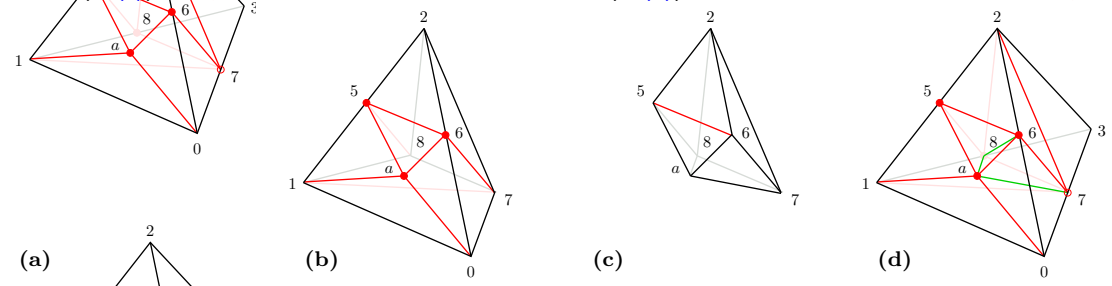


(a) (b) (c) (d)

**Figure 22**: Ambiguous case 4b$\alpha$ ($|02| = |12| < |13| < |03|$): (22(a)) constrained configuration, (22(b)) after removal of $7823$, (22(c)) after removal of $a607$, $a158$, $a017$ and $a718$, and (22(d)) complete subdivision.

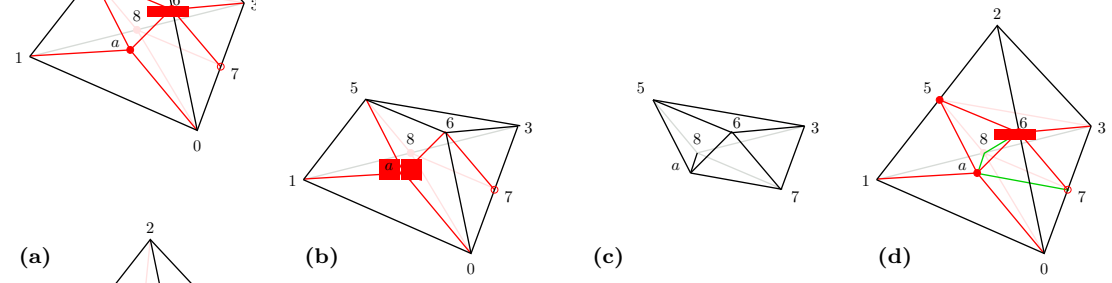


(a) (b) (c) (d)

**Figure 23**: Ambiguous case 4b$\beta$ ($|02| = |12| > |13| > |03|$): (23(a)) constrained configuration, (23(b)) after removal of $6523$, (23(c)) after removal of $a607$, $a158$, $a018$ and $a708$, and (23(d)) complete subdivision.

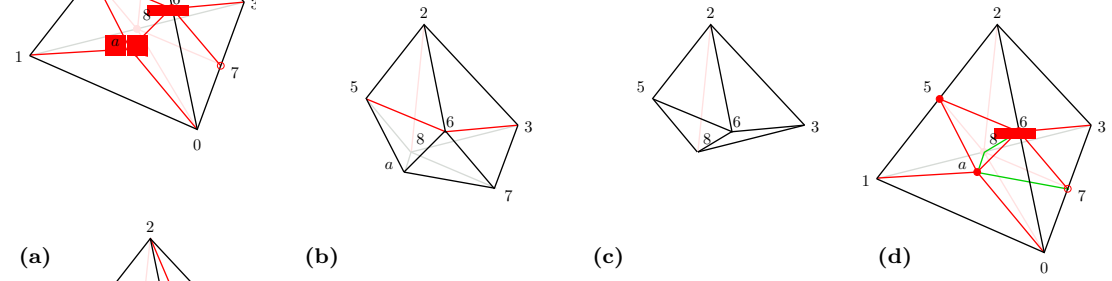


(a) (b) (c) (d)

**Figure 24**: Ambiguous case 4b$\gamma$ ($|03| < |02| = |12| < |13|$): (24(a)) constrained configuration, (24(b)) after removal of $a607$, $a158$, $a018$ and $a708$, (24(c)) after removal of $67a8$, $6a58$ and $6378$, and (24(d)) complete subdivision.

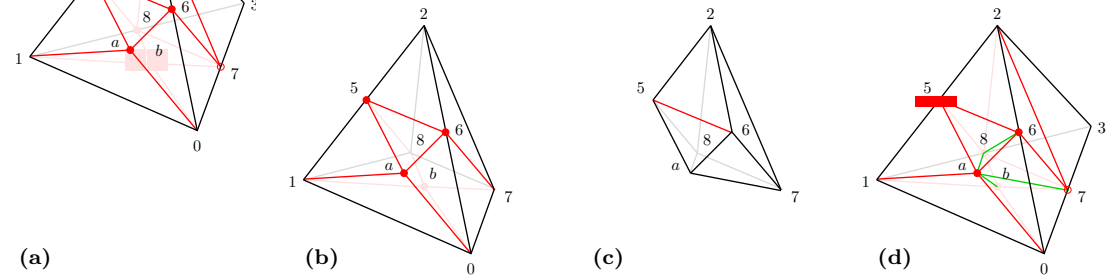


(a) (b) (c) (d)

**Figure 25**: Ambiguous case 4b$\delta$ ($|02| = |12| < |03| = |13|$): (25(a)) constrained configuration, (25(b)) after removal of $7823$, (25(c)) after removal of $a607$, $a158$, $a01b$, $ab18$, $a0b7$ and $a7b8$, and (25(d)) complete subdivision.

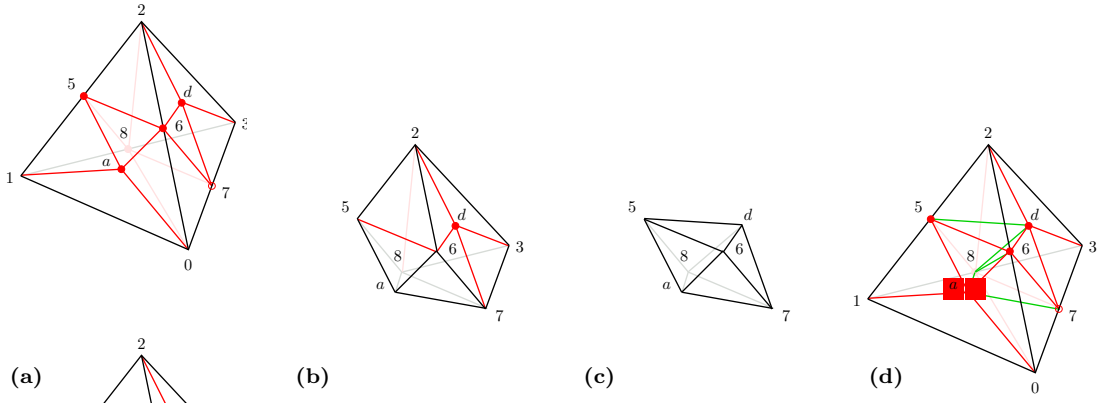

(a) (b) (c) (d)

**Figure 26**: Ambiguous case 4b$\epsilon$ ($|02| = |12| = |03| < |13|$): (26(a)) constrained configuration, (26(b)) after removal of $a607$, $a158$, $a018$ and $a708$, (26(c)) after removal of $d625$, $d378$, $d238$ and $d285$, and (26(d)) complete subdivision.

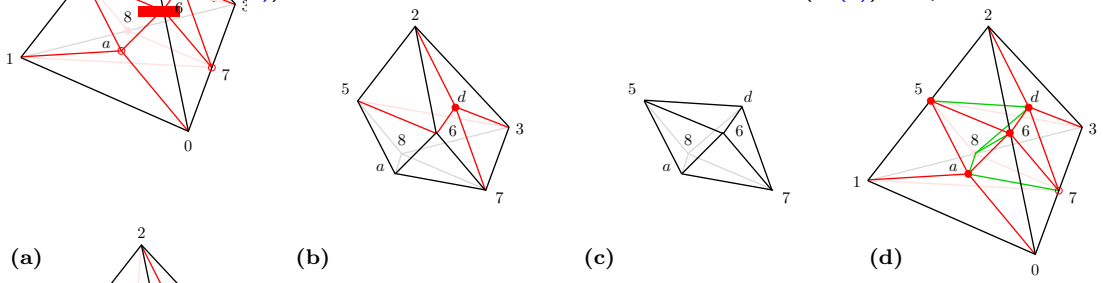

(a) (b) (c) (d)

**Figure 27**: Ambiguous case 4b$\zeta$ ($|02| = |12| = |03| > |13|$): (27(a)) constrained configuration, (27(b)) after removal of $a607$, $a158$, $a017$ and $a718$, (27(c)) after removal of $d625$, $d378$, $d235$ and $d385$, and (27(d)) complete subdivision.

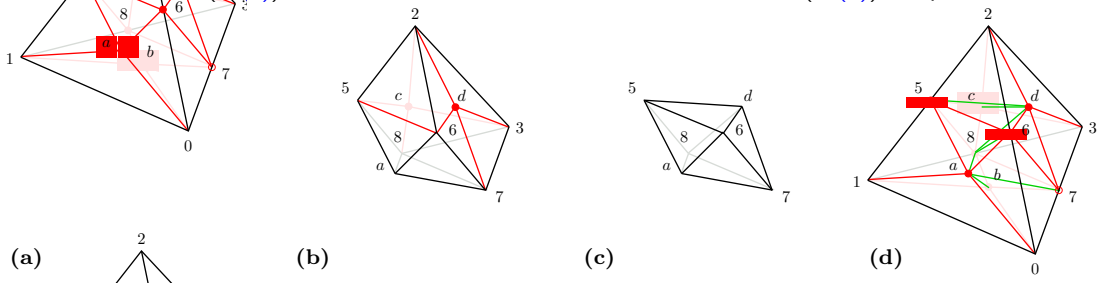

(a) (b) (c) (d)

**Figure 28**: Ambiguous case 4b$\eta$ ($|02| = |12| = |03| = |13|$): (28(a)) constrained configuration, (28(b)) after removal of $a607$, $a158$, $a01b$, $ab18$, $a0b7$ and $a7b8$, (28(c)) after removal of $d625$, $d378$, $d23c$, $d2c5$, $dc38$ and $d5c8$, and (28(d)) complete subdivision.

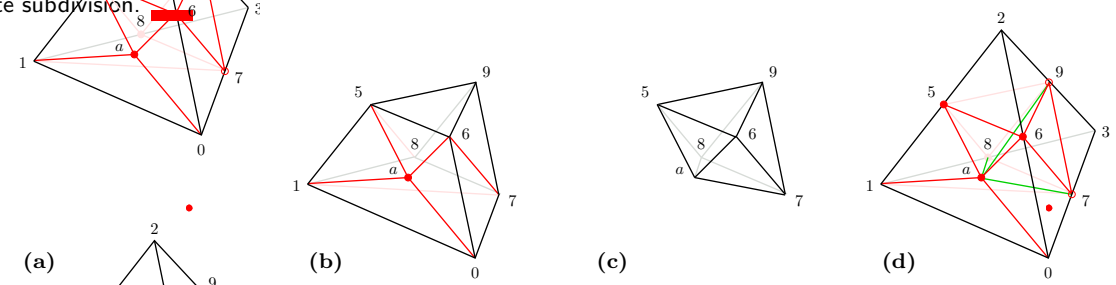

(a) (b) (c) (d)

**Figure 29**: Ambiguous case 5$\alpha$ ($|02| = |12|, |03| > |13|$): (29(a)) constrained configuration, (29(b)) after removal of $6529$ and $7893$, (29(c)) after removal of $a607$, $a158$, $a017$ and $a718$, and (29(d)) complete subdivision.

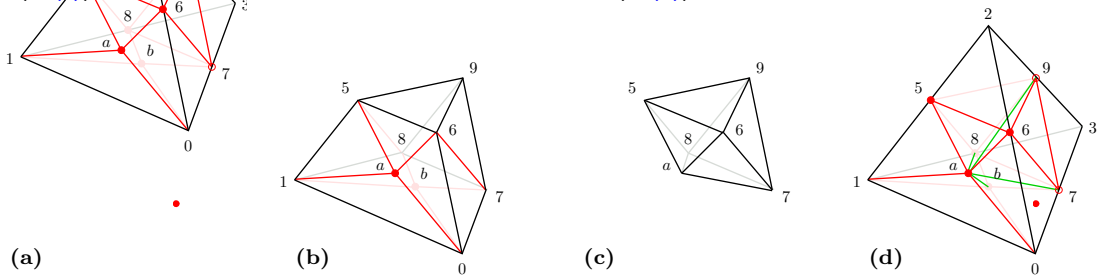

(a) (b) (c) (d)

**Figure 30**: Ambiguous case 5$\beta$ ($|02| = |12|, |03| = |13|$): (30(a)) constrained configuration, (30(b)) after removal of $6529$ and $7893$, (30(c)) after removal of $a607$, $a158$, $a01b$, $ab18$, $a0b7$ and $a7b8$, and2 (30(d)) complete subdivision.